RSC Advances

PAPER

View Article Online
View Journal | View Issue

Cite this: *RSC Adv.*, 2026, **16**, 30949

Efficient hydrogenation of furfural to furfuryl alcohol by recoverable copper tailings catalyst

Lele Shang,[abd] Weijun Dai,[c] Xiaolong Hao,[c] Dongbao Guo,[abd] Xiao Li,[d] Yongjie Niu,[abd] Yalong Yi,[abd] Hao Wang,[d] Xiaobo Pan *[c] and Shuang Dai*[ab]

Selective hydrogenation of substrates containing multiple unsaturated bonds (C=C and C=O) is a crucial catalytic process in the production of high-value chemicals. The development of non-precious metal catalytic systems is of importance for hydrogenation processes due to the high cost and scarcity of noble metals. Here, we report the direct hydrogenation of furfural (FAL) to furfuryl alcohol (FFA) over an active and stable copper tailings catalyst (CTC). The CTC showed 80% selectivity for FFA with full conversion of FAL at 200 °C under 3.0 MPa of H_2 within 72 h. Moreover, this catalyst shows good recyclability with no obvious loss in catalytic activity after five successive runs. This work uses copper tailings as an intrinsic catalyst for biomass hydrogenation, realizing the high-value utilization of industrial solid waste and providing a low-cost and sustainable catalytic system for the industrial production of biomass fine chemicals, which goes a step further towards the industrial application of heterogeneous catalysts for fine chemical production from biomass.

Received 27th February 2026
Accepted 31st May 2026

DOI: 10.1039/d6ra01723a

rsc.li/rsc-advances

1 Introduction

As the excessive consumption of fossil fuels and the growing severity of related issues such as environmental sustainability become increasingly prominent, production technologies based on renewable resources have been rapidly developed.[1–4] Biomass, as a renewable resource, is considered a unique alternative to traditional fossil energy sources, capable of yielding energy, fuels, and high-value-added chemicals. Among them, lignocellulosic biomass, due to its renewable nature and carbon neutrality, has become one of the most promising carbon sources in biomass conversion.[5–7] Furfural (FAL) is one of the main derivative products in the pyrolysis process of lignocellulosic biomass.[8] The molecular structure contains highly reactive aldehyde groups and aromatic heterocyclic functional groups, which can be transformed into high-value-added products through diverse chemical reaction pathways.[9–13] Catalytic hydrogenation is the major upgrading route for FAL (Fig. 1), leading to various valuable compounds such as furfuryl alcohol (FFA),[14–16] tetrahydrofurfuryl alcohol (THFA),[17–19] 2-methylfuran (2-MF).[20–22] FFA, a key derivative of furfural manufactured *via* hydrogenation processes, possesses exceptionally high economic value and extensive application scope.[23]

Various noble metal catalysts have been employed for the hydrogenation of FAL to FFA, mainly including Pt, Pd, Ru, and their bimetallic derivatives.[24] For example, Xiao and co-workers reported a MOF360-supported Ru catalyst that exhibited excellent performance for selective FFA production, with 98% FAL conversion and 99% FFA selectivity at 20 bar N_2 and 200 °C.[25] The PdCu-based catalyst ($PdCu/TiO_2$) developed by the Ashwani group afforded 97% FAL conversion and 99% FFA selectivity within 4 h at room temperature.[26] Similarly, Pt–PtO_x-based catalyst (Pt–PtO_x/$Mg(OH)_2$–F) gave 99.9% FAL conversion and 98.4% FFA selectivity under 20 bar of 30% H_2/N_2 at 180 °C.[27] Zhang's group developed a Pd/ZrO_2 catalyst for the catalytic transfer hydrogenation (CTH) of FAL using isopropanol (IPA) as

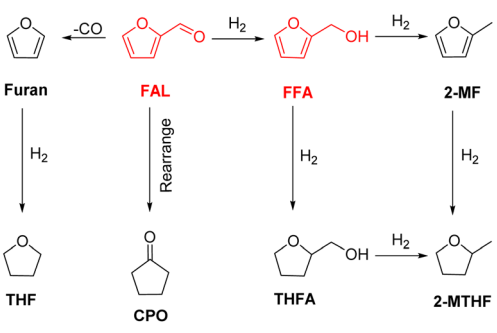

Fig. 1 Furfural and the pathway for different pathways for furfural derivatives.

[a]MNR Key Laboratory of Strategic Mineral Resources of the Upper Yellow River, School of Earth Sciences, Lanzhou University, Lanzhou 730000, China. E-mail: daisher@lzu.edu.cn

[b]MOE Key Laboratory of Western China's Environmental Systems, College of Earth and Environmental Sciences, Lanzhou University, Lanzhou 730000, China

[c]College of Chemistry and Chemical Engineering, Lanzhou University, Lanzhou 730000, China. E-mail: boxb@lzu.edu.cn

[d]Lanzhou Mineral Exploration Institute of Gansu Nonferrous Metal Geological Exploration Bureau, Lanzhou 730000, China

the hydrogen donor.[28] Although these noble metal catalysts enable high conversion and selectivity, their scarcity and high cost severely limit large-scale practical applications.

To address these limitations, extensive efforts have been devoted to exploring efficient non-noble metal catalysts from low-cost precursors. Kumar *et al.* reported that monoclinic ZrO_2 with exposed (−111) facets and abundant basic sites exhibited excellent activity and selectivity for FAL hydrogenation.[29] Liu *et al.* prepared a series of non-precious metal (Fe, Co, Ni, Cu) biochar-based catalysts and revealed that catalytic performance was mainly determined by metal valence states and dispersion.[30] Zhang *et al.* reported Cu–Al_2O_3–ZnO catalysts derived from etched Devarda's alloy, which achieved >99% FAL conversion and >99% FFA selectivity due to the synergistic effect between low-valent Cu species and acidic sites.[31] Huai *et al.* fabricated Co–N–C composites *via* surfactant-modified ZIF-67, which showed high activity and stability in selective FAL hydrogenation.[32] Xiao *et al.* further developed a highly stable Cu/MCM-41 catalyst with outstanding recyclability, which originated from the strong metal–support interaction and confinement effect of mesoporous silica.[33] Very recently, Xu *et al.* reported that Cu/Al_2O_3 catalysts with synergistic effect between Cu^0 sites and medium-strong acidic sites could achieve 100% conversion and 100% selectivity for FAL hydrogenation to FFA under mild conditions, emphasizing the crucial role of support acidity and copper valence states.[34] Nevertheless, despite the notable progress achieved above, the development and practical application of non-noble metal catalysts are still severely restricted by several inherent drawbacks.

China possesses abundant mineral resources however, long-term, and large-scale mining activities have generated massive stockpiles of tailings alongside rapid economic development. According to incomplete statistics, the total stockpile of tailings across China has surpassed 20 billion tons and continues to increase by hundreds of millions of tons annually. Such tailings not only occupy extensive land resources but also bring serious ecological and environmental hazards, including heavy metal leaching and dust pollution. Nevertheless, tailings often contain various silicate minerals, metal oxides (*e.g.*, Fe_2O_3, Al_2O_3, MgO, CaO), and trace transition metal elements, which possess potential catalytic components. In recent years, studies have attempted to use natural ores as catalyst supports for the conversion of biomass-derived furfural. However, these efforts have mostly been limited to loading active metals onto modified ores, essentially falling within the scope of traditional supported catalysts.[35–38] Notably, to date, there have been no reports on the direct use of unmodified copper tailings as intrinsic catalysts for catalytic hydrogenation conversion of biomass.

Herein, we propose a stable, low-cost, and reusable copper tailings catalyst (CTC) for the selective catalytic hydrogenation of FAL to FFA, which breaks the limitation of tailings only as catalyst supports and realizes the direct conversion of industrial solid waste to catalytic active materials. The catalyst is directly prepared by calcination of CTC in a muffle furnace followed by H_2/Ar reduction in a tube furnace. Under the conditions of an initial hydrogen pressure of 3.0 MPa, a temperature of 200 °C, and IPA as the solvent, the CTC achieved a furfural conversion rate of 100% and a FFA selectivity of 80% after 72 h of reaction. Notably, this CTC catalyst exhibits broad substrate universality for the hydrogenation of various substituted aldehydes, and can be recycled for five times without significant loss of catalytic performance, solving the problem that non-precious metal catalysts are difficult to balance activity, selectivity, and recyclability. This method may lay the foundation for developing novel catalysts, which are expected to find applications in sustainable catalysis and open a new path for the resource utilization of tailings solid waste.

2 Experimental section

2.1 Materials

FAL (AR, 99%), FFA (98%), THFA (AR, 99%), 5-hydroxymethylfurfural (HMF) (96%), cinnamaldehyde (98%), *n*-tridecane (AR, 99%), 5-nitrofurfural (98%), 4-bromobenzaldehyde (AR, 99%), 4-chlorobenzaldehyde (97%), 3-iodobenzaldehyde (98%), benzaldehyde (AR, 99%), *p*-tolualdehyde (98%), *p*-anisaldehyde (AR, 99%), 4-fluorobenzaldehyde (98%), 3-bromobenzaldehyde (97%), 2-bromobenzaldehyde (98%), 3-methoxybenzaldehyde (98%), *m*-tolualdehyde (95%), 4-hydroxybenzaldehyde (AR, 99%), 4-(trifluoromethyl)benzaldehyde (98%) and 5-methyl furfural (98%) were purchased from Energy Chemical (Saan Chemical Technology (Shanghai) Co., Ltd, China). IPA (AR, 99%), CH_3OH (AR, 99%), ethanol (AR, 99%), THF (AR, 99%), toluene (AR, 99%), $Ni(NO_3)_2 \cdot 6H_2O$ (AR, 99%), $Cu(NO_3)_2 \cdot 3H_2O$ (AR, 99%) and $Zn(NO_3)_2 \cdot 6H_2O$ (AR, 99%) were obtained from Chengdu Chron Chemical Co., Ltd $Co(NO_3)_2 \cdot 6H_2O$ (AR, 99%) were purchased from Shanghai Macklin Biochemical Co., Ltd $Fe(NO_3)_3 \cdot 9H_2O$ (AR, 99%) was provided by Saan Chemical Technology (Shanghai) Co., Ltd. All chemicals were used without further purification.

2.2 Catalyst preparation

2.2.1 Preparation of CTC. The copper tailing raw material used for preparing CTC was collected from the copper system tailings of the No. 2 Tailings Pond of Baiyin Concentrator in Gansu Province, with the sampling location at 104°15′34″ E longitude and 36°34′25″ N latitude. Copper tailings sand was dried in an oven at 60 °C for 12 h. The dried sand was ground in a rod mill for 4 h to yield a 100-mesh CTC precursor. Then, the precursor was subjected to H_2/Ar reduction treatment in a tube furnace under the conditions of 350 °C for 6 h. Finally, the target CTC was obtained.

2.2.2 Preparation of copper tailings composite catalysts. The preparation of copper tailings-based composite catalysts *via* the impregnation method mainly involves pre-treatment of the copper tailings support, preparation of an impregnation solution containing precursor compounds of metal active components (Ni, Cu, Zn, Co, Fe), loading by incipient wetness impregnation, static aging, drying in a blast drying oven, programmed temperature calcination in a muffle furnace, followed by activation and reduction in a tube furnace, ultimately yielding highly dispersed copper tailings-based composite catalysts.

2.3 Catalyst characterization

The crystal structure of the sample was characterized by X-ray powder diffraction (XRD) using a Shimadzu XRD-6100 instrument. N_2 adsorption–desorption isotherms were measured with a JW-BK200C analyser. Elemental composition was determined by Agilent 7850 ICP-MS. Scanning electron microscopy (SEM) coupled with energy-dispersive X-ray spectroscopy (EDS) for atomic identification was performed using a CIQTEK SEM 3200 electron microscope. TEM was conducted using JEM-2100 at 200 kV. HAADF-STEM images and elemental mappings were obtained *via* Talos F200X G2. The surface elemental chemical states of the catalysts were analysed by X-ray photoelectron spectroscopy (XPS) on a Thermo Fisher Nexsa G2 spectrometer. Hydrogen temperature-programmed reduction (H_2-TPR) and hydrogen temperature-programmed desorption (H_2-TPD) experiments were carried out on a Micromeritics AutoChem II 2920 automated chemisorption analyser equipped with a thermal conductivity detector (TCD). Thermogravimetric analysis (TG or TGA) of residual weight loss in CTC samples was conducted using a TGA/DSC3+/Sartorius/MCA125S-2CCN-1 system. Detailed experimental parameters and procedures are provided in the SI.

2.4 Evaluation of catalytic performance

The hydrogenation of FAL-derived FFA over CTC catalysts was carried out in a 50 mL magnetic stirred high-pressure reactor vessel. Prior to testing, the catalyst was reduced at 350 °C for 6 h. The catalyst (0.50 g), substrate (1.0 mmol), and IPA (10 mL) were sequentially added to the reactor vessel and purged with hydrogen for 3–5 cycles. Subsequently, 3.0 MPa H_2 was introduced, and after ensuring air-tightness, the heating and stirring devices (700 rpm) were activated to initiate the reaction, thereby ensuring uniform mass and heat transfer. After completion of the catalytic reaction, the samples were subjected to qualitative analysis using gas chromatography-mass spectrometry (Thermo TRACE 1300-ISQ LT GC-MS) and quantitative analysis using gas chromatography (Agilent 7890B), with *n*-tridecane as the internal standard. In the cycling stability test, the spent catalyst was washed repeatedly with deionized water and ethanol, dried at 120 °C in an oven, and then reused for the subsequent reaction over five consecutive cycles. The conversion (Con.%), product selectivity (Sel.%), and yield were calculated as the following formulas:

$$\text{Con.}/\% = \frac{n_{a,0} - n_a}{n_{a,0}} \times 100\% \quad (1)$$

$$\text{Sel.}/\% = \frac{w_i}{\sum w_i} \times 100\% \quad (2)$$

$$\text{Yield}/\% = \frac{n_a}{n_{a,0}} \times 100\% \quad (3)$$

To confirm the phase state of the reaction system, we calculated the saturated vapor pressures of isopropanol solvent and furfural substrate *via* the Antoine method. Relevant thermodynamic constants were selected from standard databases. At 200 °C, the saturated vapor pressure of isopropanol was calculated to be 2.58 MPa, while that of furfural was 1.56 MPa. Given that the actual reaction pressure was set at 3 MPa, which exceeds the saturated vapor pressure of isopropanol, the volatilization of reaction components was effectively inhibited. Consequently, the whole reaction system existed stably in the liquid phase throughout the transfer hydrogenation reaction.

3 Results and discussion

3.1 Chemical composition of the CTC used in the experiments

Perform chemical analysis and process mineralogical characterization on the obtained copper tailings samples. The product fineness for the flotation feed in an industrial flotation circuit was around 70 wt% passing through 200 mesh. The main recoverable valuable element in the ore samples was copper. Its content was reduced to 1826 mg kg^{-1} after the flotation process, as determined by Inductively Coupled Plasma Mass Spectrometry. In addition, the copper tailings sample contained predominantly 66.70 wt% SiO_2 along with 12.40 wt% Fe_2O_3, 6.76 wt% Al_2O_3 and 3.86 wt% MgO (Fig. 2a). Remarkably, traditional engineered Cu-based catalysts typically require 5–20 wt% Cu loading to achieve satisfactory hydrogenation activity. Recent literature indicates that Fe_2O_3 can promote H_2 spillover, while the amphoteric nature of Al_2O_3 and MgO provides essential acid–base sites to polarize the C=O bond of furfural, synergistically enhancing the intrinsic activity of the highly dispersed trace copper. This likely contributes to CTC's high hydrogenation activity.

3.2 Structural properties of CTC

Further compositional analysis of the CTC using the XRD pattern reveals that the catalyst is primarily composed of quartz, clay minerals, plagioclase, pyrite, and a small amount of calcite. Fig. 2b also provides the content of each mineral component, thus the XRD analysis results of the CTC and the elemental

(a) Major elements, %

SiO_2	Fe_2O_3	Al_2O_3	MgO	CaO	K_2O	Na_2O	TiO_2	MnO	P_2O_5
66.70	12.40	6.76	3.86	0.74	0.65	0.34	0.06	0.04	0.02

Trace elements, mg/kg

Cu	Zn	Ba	Zr	Cr	V	Rb	Sr	Ni
1826	1324	546	221	27	17	10	27	8

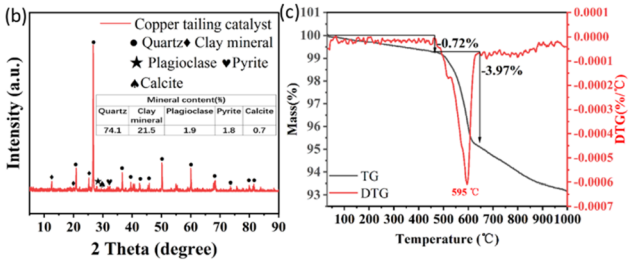

Fig. 2 (a) Chemical composition of the CTC used in the experiments. (b) XRD pattern of CTC. (c) TG analysis of CTC.

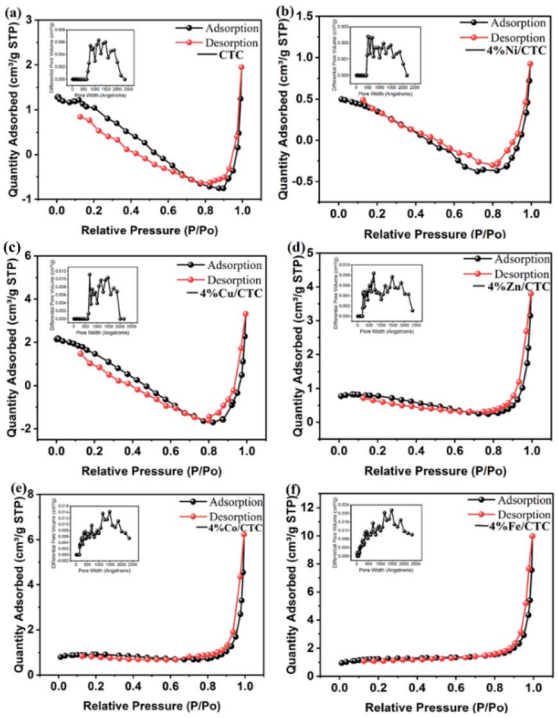

Fig. 3 Nitrogen adsorption isotherms and pore size distribution of CTC (a), 4% Ni/CTC (b), 4% Cu/CTC (c), 4% Zn/CTC (d), 4% Co/CTC (e) and 4% Fe/CTC (f).

analysis results can mutually corroborate one another. Regarding the XRD quantitative analysis of CTC, Rockquan 2018 software was used strictly in accordance with the industry standard SY/T 5163-2018. The full pattern summation method combined with the reference intensity ratio (RIR) method was adopted for mineral quantification, in which all mineral contents were calculated from the fitted full-spectrum diffraction intensities and the built-in standard RIR values of each mineral phase, and the results were automatically normalized to 100 wt%.

TG analysis of CTC at intervals was carried out to study the weight losses, which aimed at giving more confirming insights into the evidence obtained by XRD analysis. Result of TG analysis was indicated in Fig. 2c. Fig. 2c indicated two separated stages of weight loss in CTC. Volatilized chemical binding water of CTC may be responsible for the beginning stage within 500 °C. Release of CO_2 originated from carbonate can explain weight loss at temperature between 500 °C and 650 °C. The relatively high temperature range indicates that the catalyst exhibits good thermal stability below 500 °C, making it suitable for medium to high-temperature reaction environments.

Since specific surface area and pore size distribution are key structural parameters that regulate catalyst performance, they profoundly influence mass transfer efficiency of reactants and products, active-site exposure, and adsorption capacity. Brunauer–Emmett–Teller (BET) tests were therefore conducted to characterize the textural properties of all samples. Fig. 3 shows N_2 adsorption–desorption isotherms and pore size distribution curves of CTC, 4% Ni/CTC, 4% Cu/CTC, 4% Zn/CTC, 4% Co/CTC and 4% Fe/CTC. Clearly, all samples exhibit a type III hysteresis loop as classified by IUPAC, which suggests the presence of a mesoporous structure in the samples. The pore size distribution curve further proves the mesoporous structures.

Textural parameters, including BET specific surface area, pore volume, and average pore size, for the bare CTC support and various 4% metal-loaded CTC catalysts are summarized in Table 1. The raw CTC support exhibits a low surface area of 1.97 $m^2\ g^{-1}$, a pore volume of 3.01×10^{-3} $cm^3\ g^{-1}$, and an average pore size of 61.01 nm. After metal impregnation, significant changes in the porous structure are observed. Notably, the 4% Ni/CTC catalyst shows a substantial decrease in both surface area (0.55 $m^2\ g^{-1}$) and pore volume (1.42×10^{-3} $cm^3\ g^{-1}$), accompanied by an increase in pore size to 102.66 nm. In contrast, catalysts loaded with Cu, Co, and Fe show enhanced surface areas compared to the bare support, with 4% Fe/CTC exhibiting the highest value at 3.90 $m^2\ g^{-1}$. Pore volumes generally increase with metal loading, reaching a maximum of 1.54×10^{-2} $cm^3\ g^{-1}$ for 4% Fe/CTC. The average pore size also tends to increase upon metal incorporation, with the 4% Fe/CTC catalyst displaying the largest pore diameter at 158.27 nm. These variations indicate that the introduction of different metals significantly alters the porous structure of the CTC support, likely due to metal deposition within pores, structural rearrangement, or the creation of new porosity.

Fig. 4 presents the morphological, microstructural, and elemental distribution characteristics of the as-prepared CTC catalyst. The low-magnification SEM image (Fig. 4a) shows that the raw CTC powder consists of polydisperse, irregularly shaped particles with a wide size distribution, ranging from submicrometer to hundreds of micrometers. This heterogeneous morphology is typical of natural mineral tailings, resulting from the complex ore beneficiation processes and multi-phase

Table 1 Textural properties of the CTC support and various 4% metal-loaded CTC catalysts (Ni, Cu, Zn, Co, Fe)

Catalyst	Surface area[a] ($m^2\ g^{-1}$)	Pore volume[a] ($cm^3\ g^{-1}$)	Pore size[a] (nm)
CTC	1.97	3.01×10^{-3}	61.01
4% Ni/CTC	0.55	1.42×10^{-3}	102.66
4% Cu/CTC	2.33	5.12×10^{-3}	87.74
4% Zn/CTC	1.89	5.87×10^{-3}	123.66
4% Co/CTC	2.55	9.64×10^{-3}	150.99
4% Fe/CTC	3.90	1.54×10^{-2}	158.27

[a] BET surface area.

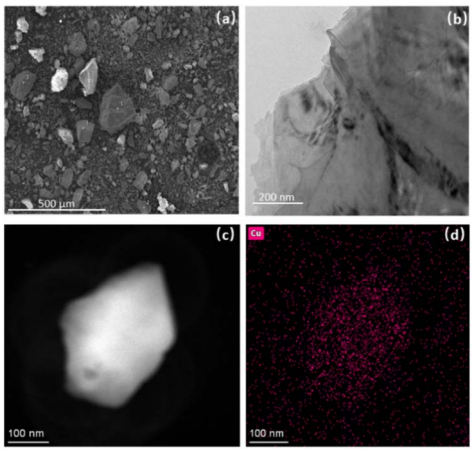

Fig. 4 (a) SEM image of CTC, (b) TEM image of CTC, (c and d) HAADF-STEM image and corresponding EDS mapping images of Cu over CTC sample.

mineral composition. To further investigate the nanoscale structure and active species distribution, high-resolution TEM was performed (Fig. 4b). The TEM image reveals layered crystalline domains corresponding to the silicate matrix of the tailings, along with fine, dispersed dark spots assigned to Cu-based active species. The high dispersion of these Cu sites, embedded within the mineral framework, is essential for achieving high activity in furfural hydrogenation, as it ensures a high density of accessible active sites. Additionally, the presence of structural defects and grain boundaries in the matrix is evident, which may contribute to enhanced mass transfer and reactant adsorption properties.

The morphology and elemental distribution of the 4% Cu/CTC catalyst were characterized by HAADF-STEM and corresponding EDS mapping. Fig. 4c presents the HAADF-STEM image of a representative catalyst particle, revealing a relatively dense, irregularly shaped structure with a size of several hundred nanometers. The corresponding Cu elemental mapping (Fig. 4d) shows that Cu species are homogeneously distributed throughout the entire catalyst particle, with a higher density of signals observed within the region corresponding to the bright particle in the STEM image. This confirms the successful loading and uniform dispersion of Cu on the CTC support, which is critical for the catalytic performance.

To verify the chemical valence state and existing form of copper species in the as-prepared catalyst, XPS characterization was performed, and the high-resolution Cu 2p spectrum is presented in Fig. S10. The Cu 2p region exhibits the characteristic spin–orbit split doublet, consisting of Cu $2p_{3/2}$ (lower binding energy) and Cu $2p_{1/2}$ (higher binding energy) signals with a separation of approximately 19.8 eV, and deconvolution of the spectrum reveals two distinct sets of components: the blue-shaded components centered at 934–935 eV (Cu $2p_{3/2}$) and 954–955 eV (Cu $2p_{1/2}$) are assigned to Cu^{2+} species, while the red-shaded components located at lower binding energies of 932–933 eV (Cu $2p_{3/2}$) and 952–953 eV (Cu $2p_{1/2}$) are attributed to reduced copper species (Cu^{+}/Cu^{0}). Quantitative analysis based on the integrated peak areas reveals that reduced copper species (Cu^{+}/Cu^{0}) dominate the surface copper composition despite the extremely low total Cu loading of 0.15 wt%, confirming the presence of catalytically relevant reduced Cu sites on the catalyst surface and providing direct spectroscopic evidence for the active copper species responsible for the target reaction.

3.3 Hydrogenation of furfural over CTC

3.3.1 The effect of reaction parameters. Fig. 5a illustrates that as the reaction temperature increased from 150 °C to 210 °C, the conversion of FAL rose from 65% to 98%. During this temperature ramp, the selectivity for FFA increased from 6% to 80% within the range of 150–200 °C, but declined to 51% when the temperature was further elevated to 210 °C. These results confirm 200 °C as the optimal reaction temperature. Notably, only 65% FAL conversion and 6% FFA selectivity were attained at 150 °C, highlighting the critical role of temperature in regulating both reaction efficiency and product selectivity. Furthermore, the elevated temperature of 210 °C triggers additional side reactions (*e.g.*, over-hydrogenation of FFA to tetrahydrofurfuryl alcohol), which directly contributes to the significant drop in FFA selectivity.

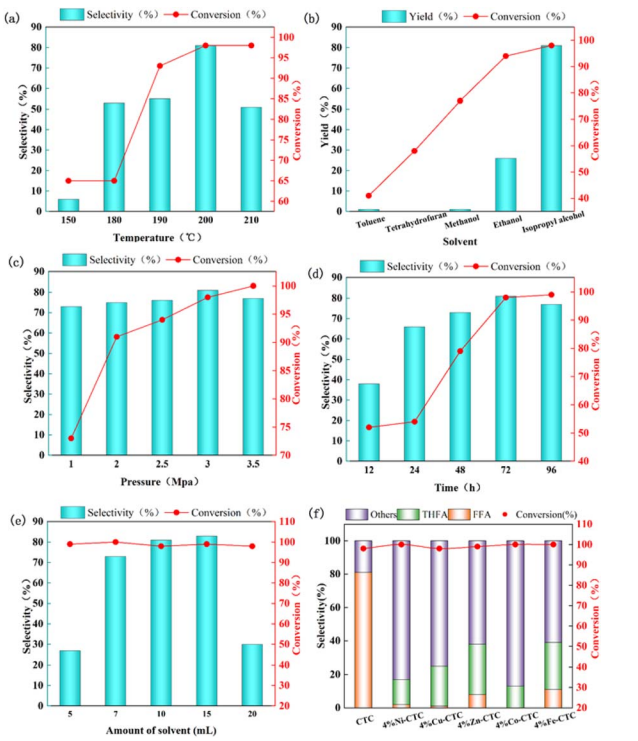

Fig. 5 Catalysis performance for the hydrogenation of FAL over CTC. Effects of (a) reaction temperature, (b) reaction solvent, (c) H_2 pressure, (d) reaction time, (e) amount of reaction solvent, and (f) composite CTC for furfural hydrogenation. Reaction conditions: 1 mmol FAL, 0.50 g catalyst with (a) 150–210 °C, 3 MPa H_2, 72 h, (b) 200 °C, 3 MPa H_2, with different solvents, 72 h, (c) 200 °C, 1–3.5 MPa H_2, 72 h, and (d) 200 °C, 3 MPa H_2, 12–96 h, (e) 200 °C, 3 MPa H_2, 72 h, 5–20 mL, (f) 200 °C, 3 MPa H_2, 72 h.

To elucidate the specific role of solvents in the hydrogenation of furfural, a range of organic solvents, alongside water, was subjected to testing. As shown in Fig. 5b, at 3.0 MPa H_2 pressure, the CTC has almost no activity in THF, relatively low conversion in methanol and toluene, but achieves a conversion of >95% in IPA. In ethanol, the conversion rate of furfural exceeds 90%, and the yield of the target product FFA is only 26%. This gives rise to the hypothesis that a portion of the hydrogen necessary for hydrogenation is derived from the unique characteristics of branched alcohols. Specifically, IPA likely acts not merely as a solvent, but actively participates as a hydrogen donor *via* a Meerwein–Ponndorf–Verley (MPV) CTH mechanism. Under 3.0 MPa H_2, a competitive and synergistic regime between direct H_2 hydrogenation and IPA-mediated CTH exists. The high pressure of molecular H_2 suppresses excessive CTH side pathways, such as rapid acetone accumulation and etherification, thereby optimizing FFA selectivity.

It is still a challenge to achieve a high yield to FFA over hydrogenation of furfural over CTC under mild conditions. We investigated the effect of initial H_2 pressure on the conversion rate and product yield of furfural. As shown in Fig. 5c, within the range of H_2 pressures from 1 to 3.5 MPa, there are significant differences in the selectivity of products. At 1 MPa, although the conversion rate of furfural reaches 74%, many by-products are produced, with a selectivity of only 56%. As the pressure increases, the conversion rate of FAL continues to increase. Compared to 3.5 MPa, the conversion rate of FAL slightly decreases at 3.0 MPa, but the selectivity of FFA remains the highest at 80%, and the formation of by-products is significantly reduced. At higher pressures, the conversion rate of FAL and the yield of FFA remain almost unchanged. This indicates that under low pressure, the dehydrogenation ability of IPA can be improved, but more by-products will also be produced. Higher H_2 pressure inhibits the dehydrogenation of IPA and no longer significantly influences the catalytic activity (Fig. 5d). The FAL conversion and the FFA selectivity increased with an increase in the reaction time from 12 h to 96 h. When the reaction time is 72 h, a furfural conversion rate of 98% and a FFA selectivity of 80% can be achieved. If the reaction time is further shortened to 12 h, the catalyst activity will drop significantly. When the reaction time is increased to 96 h, side reactions will occur and the selectivity of FFA will decrease. It is critical to compare this kinetics with reported literature. While recent highly engineered non-noble metal catalysts, such as etched Cu–Al_2O_3–ZnO or highly dispersed Cu/SiO_2, can achieve >95% FFA yield within 2–4 h at <150 °C, the CTC requires a prolonged reaction time (72 h) and higher temperature (200 °C). This kinetic limitation is directly attributed to the ultra-low absolute density of active Cu sites (0.18 wt%). Furthermore, the high temperature (200 °C) required to overcome this kinetic barrier inherently triggers consecutive side reactions, such as the hydrogenation of FFA to 2-methylfuran or etherification with the solvent, which explains the thermodynamic ceiling of 80% maximum FFA selectivity observed in this batch system. In the exploration of solvent dosage (Fig. 5e), 99% FAL conversion with 83% FFA selectivity and 98% FAL conversion with 80% FFA selectivity can also be accomplished by dosing 15 mL and 10 mL solvent, respectively. However, when the solvent volume was 5 mL or 20 mL, the selectivity for furfural alcohol would significantly decrease.

Table 2 Performance comparison of existing catalysts

Entry	Catalyst	Conv. (%)	Sel. (%)	Ref.
1	CTC	98	80	This work
2	PdCu/Al_2O_3	40	99	33
3	Co@C–N	100	85.6	34
4	PdCo/CNTs-DES-40	100	99	35
5	PdAg	100	97.1	36
6	Pt/WN–TiO_2	97.8	98.6	37
7	Cu/SBA-15	99.3	99	38
8	Cu/SiO_2	55.2	99.9	39
9	Cu/ZrO_2	85.9	100	40
10	Cu/Al_2O_3	99.9	99.9	41
11	Cu/MgO–La_2O_3	99.9	99.9	42

Achieving high selectivity towards FFA under mild conditions, while avoiding the over-hydrogenation of FAL to THFA, remains a current challenge. As shown in Fig. 5f, we compared the hydrogenation results at 200 °C, in IPA solvent, under 3 MPa H_2 pressure, using copper tailings loaded with different metals (4% Ni/CTC, 4% Cu/CTC, 4% Zn/CTC, 4% Co/CTC, 4% Fe/CTC). When the 4% Cu/CTC was used, FAL conversion reached 98% with a FFA selectivity of 80%. In contrast, when other copper tailings composite catalysts were employed, although full conversion (100%) was achieved, all reactions exhibited over-hydrogenation. This resulted in the products containing both FFA and THFA, leading to significantly diminished reaction selectivity.

In Table 2, we summarize the catalytic performance of several existing catalysts (PdCu/Al_2O_3, Co@C–N, PdCo/CNTs-DES-40, PdAg, Pt/WN–TiO_2, Cu/SBA-15, Cu/SiO_2, Cu/ZrO_2, Cu/Al_2O_3 and Cu/MgO–La_2O_3) for the conversion of furfural to furfuryl alcohol, and compare them with our prepared CTC.[39–48] We found that except for PdCu/Al_2O_3 which exhibits a relatively low conversion rate, the other catalysts achieve nearly 99% conversion with furfuryl alcohol selectivity exceeding 80%. Compared to these catalysts, our catalyst is more cost-effective and features a straightforward preparation process.

3.3.2 Reusability and universality of CTC. Furthermore, the substrate universality of the CTC catalyst was investigated for catalytic hydrogenation of various substituted aldehydes under same reaction conditions and their results are presented in Table 3. The CTC exhibited high conversion rates (>70%) for the hydrogenation of all tested aldehydes bearing substituents. Under conditions of 200 °C, HMF was selectively converted to 23% 2,5-bis(hydroxymethyl)furan (BHMF) over 72 h, whereas the conversion rate reached approximately 73% for the substrate 5-methylfurfural. For cinnamaldehyde, the CTC achieved significantly improved conversion (>90%) and FFA selectivity (>85%). It is noteworthy that this catalyst achieved exceptionally high conversion and selectivity in the hydrogenation of benzaldehyde to benzyl alcohol. Furthermore, its performance in converting substituted benzaldehydes also yielded outstanding conversion rates and selectivity.

Table 3 Substrate scope studies for the catalytic transfer hydrogenation of various furfural derivatives over CTC[a]

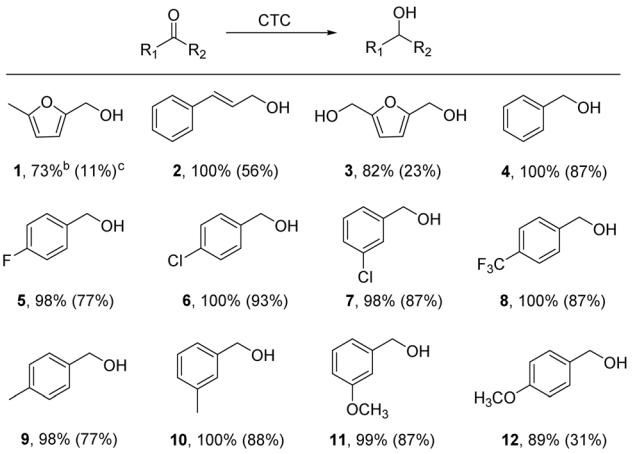

[a] Reaction conditions: 1 mmol substrate, 10 mL IPA, 0.50 g CTC, 200 °C, 3.0 MPa H_2, 72 h. [b] Aldehyde conversion. [c] Alcohol selectivity.

In addition to the high catalytic activity, the long-term stability of catalysts is also very important. Thus, the recyclability of CTC was examined at 200 °C in 72 h reaction time and in the presence of 3.0 MPa H_2. Compared with homogeneous catalytic systems, the CTC catalyst in the experimental catalytic system can be separated from the reaction mixture *via* centrifugation, washed multiple times with deionized water and ethanol, dried in an oven at 120 °C, and subsequently subjected to the next cycle of testing under identical reaction conditions, as illustrated in Fig. 6.

To further evaluate its industrial application potential in furfural conversion, the recycling stability and regeneration performance of the CTC catalyst were specifically investigated, as shown in Fig. 6a. The FAL conversion remained at nearly 100% over the first five consecutive reaction cycles, suggesting that no significant irreversible deactivation of the active sites occurred during repeated use. In contrast, the selectivity toward the target product exhibited a clear declining trend with increasing cycle numbers, dropping from approximately 81% in the first run to around 38% in the fifth run. This decrease is likely attributed to the coverage of active sites by by-products or carbonaceous deposits, changes in the valence state of metal species, or partial agglomeration during the reaction. After the fifth cycle, the spent catalyst was subjected to a regeneration treatment (*e.g.*, calcination or reduction). As observed in the sixth run, the selectivity recovered to about 81%, nearly returning to its initial value. This result confirms that the selectivity decay is reversible, and the catalytic performance can be effectively restored through simple regeneration, highlighting the catalyst's promising prospects for industrial recycling.

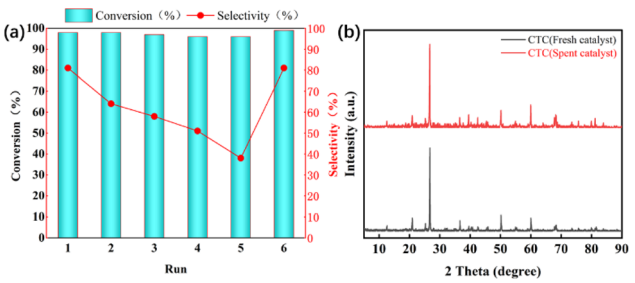

Fig. 6 (a) Recyclability test in the hydrogenation of FAL to FFA. 1.0 mmol furfural, 0.50 g CTC, 10 mL IPA, 3.0 MPa H_2, 200 °C, 72 h. (b) XRD profiles of pristine and used CTC copper tailings catalyst.

To further explore the structural stability of the catalyst, XRD characterization was performed on both the fresh and spent CTC catalysts, as presented in Fig. 6b. No obvious shifts in the positions of the characteristic diffraction peaks were observed after the reaction, and no new impurity peaks appeared. These findings indicate that the main crystalline phase of the CTC catalyst was not destroyed during reaction and regeneration. The slight variations in the intensity of some diffraction peaks may be related to changes in the crystallinity of the metal active species or minor carbon deposition on the catalyst surface, which is also consistent with the decrease in selectivity observed in the recycling tests.

The effect of reaction atmosphere on the catalytic performance of CTC for FAL hydrogenation was investigated, and the results are shown in Table S1. Under 3.0 MPa H_2 atmosphere, the conversion of furfural reached 98%, with 80% selectivity to FFA and no formation of THFA. In sharp contrast, under 3.0 MPa N_2 atmosphere, the conversion of FAL was only 2%, and no target products (FFA or THFA) were detected, with all products being unidentified by-products. These results clearly demonstrate that external H_2 is the essential hydrogen source for this reaction, and that IPA cannot act as an effective hydrogen donor for furfural hydrogenation over the CTC catalyst under the tested conditions.

3.4 Mechanistic aspects

Based on literature study, the different product distribution over catalyst in the FAL hydrogenation, the possible reaction mechanism is outlined (Fig. S9).[49–53] FAL adsorbed onto the CTC surface and subsequently undergoes multiple intermediate

steps to generate various products. The adsorption of FAL is stronger on CTC surface. Therefore, hydrogenation of carbonyl group of the adsorbed FAL to generate a hydroxyalkyl intermediate, followed by hydrogenation of carbon bearing hydroxyl group to form FFA that was observed over the catalysts.

The FAL may undergo a series of internal reaction pathways including hydrogenation, dehydrogenation, and decarbonylation to form a different product, making it difficult to find the exact path for the formation of each product. The conversion of FAL to FFA features a lower reaction barrier, making it kinetically favourable under specific H_2 coverage, temperature, and pressure conditions.

4 Conclusions

In summary, we investigated the use of CTC for the selective hydrogenation of FAL to FFA and optimized the relevant reaction parameters. Complete conversion of FAL with 80% FFA selectivity was achieved under the optimized conditions of 200 °C and 30 bar hydrogen pressure within 72 h, and IPA was identified as the preferred solvent for promoting the hydrogenation reaction. This work is the first to report the use of unmodified copper tailings as an intrinsic catalyst for the selective hydrogenation of furfural, which is a key innovation in the design of biomass hydrogenation catalysts, realizing the high-value utilization of industrial tailings solid waste with both environmental and economic benefits. The catalyst's reusability was successfully tested over five consecutive operational cycles without significant performance degradation, solving the long-standing problem that traditional non-precious metal catalysts cannot balance catalytic activity, product selectivity and cycling stability. Furthermore, the CTC catalyst exhibits excellent substrate universality, which can efficiently catalyse the selective hydrogenation of various furfural derivatives, aromatic aldehydes, and substituted benzaldehydes to the corresponding alcohols, expanding the substrate range of biomass aldehyde hydrogenation. Additionally, comparisons with other reported catalysts demonstrated the catalyst's broad commercial potential in the design of biomass chemical conversions to industrially applicable products. This study provides a low-cost, noble metal-free and sustainable catalytic system for the catalytic conversion of biomass, and opens a new direction for the resource utilization of industrial tailings solid waste, which has important guiding significance for the development of green and sustainable biomass catalysis technology.

Author contributions

Lele Shang: conceptualization, methodology, formal analysis, investigation, writing – original draft. Weijun Dai: conceptualization, methodology, supervision. Xiaolong Hao: conceptualization, supervision, writing – review & editing. Dongbao Guo: data curation, supervision. Xiao Li: conceptualization, methodology, supervision. Yongjie Niu: validation, data curation, formal analysis. Yalong Yi: validation, data curation. Hao Wang: validation, data curation. Xiaobo Pan: validation, data curation, formal analysis. Shuang Dai: validation, data curation, formal analysis.

Conflicts of interest

There are no conflicts to declare.

Data availability

Supplementary information (SI) is available. See DOI: https://doi.org/10.1039/d6ra01723a.

Acknowledgements

This work were supported by Gansu Nonferrous Metal Geological Exploration Bureau managed projects (YSJG2024-02) and Gansu Provincial Department of Science and Technology (24YFGA019).

Notes and references

1 K. R. Abbasi, M. Shahbaz, J. Zhang, M. Irfan and R. Alvarado, *Renewable Energy*, 2022, **187**, 390.
2 J. Wang and W. Azam, *Geosci. Front.*, 2024, **15**, 101757.
3 M. Stöcker, *Angew. Chem., Int. Ed.*, 2008, **47**, 9200.
4 D. Carpenter, T. L. Westover, S. Czernik and W. Jablonski, *Green Chem.*, 2014, **16**, 384.
5 J. Gan, L. Chen, Z. Chen, J. Zhang, W. Yu, C. Huang, Y. Wu and K. Zhang, *Small*, 2023, **19**, 2304066.
6 F. Wang, D. Ouyang, Z. Zhou, S. J. Page, D. Liu and X. Zhao, *J. Energy Chem.*, 2021, **57**, 247.
7 L. Cherwoo, I. Gupta, G. Flora, R. Verma, M. Kapil, S. K. Arya, B. Ravindran, K. S. Khoo, S. K. Bhatia, S. W. Chang, C. Ngamcharussrivichai and V. Ashokkumar, *Sustain. Energy Technol. Assessments*, 2023, **60**, 103563.
8 K. J. Yong, T. Y. Wu, C. B. T. L. Lee, Z. J. Lee, Q. Liu, J. M. Jahim, Q. Zhou and L. Zhang, *Biomass Bioenergy*, 2022, **161**, 106458.
9 Y. Wang, D. Zhao, D. Rodríguez-Padrón and C. Len, *Catalysts*, 2019, **9**, 796.
10 S. Yu, Y. Shi, D. Liu, Q. Gao, X. Li, C. Feng, P. Dai, L. Li, X. Gu and Y. Liu, *Appl. Surf. Sci.*, 2025, **700**, 163225.
11 F. Wang, Z. Duan, K. Zhao, Z. Xiao and X. Liu, *Ind. Eng. Chem. Res.*, 2025, **64**, 13024.
12 W. Lin, Y. Chen, Y. Zhang, Y. Zhang, J. Wang, L. Wang, C. C. Xu and R. Nie, *ACS Catal.*, 2023, **13**, 11256.
13 X. Yang, Z. Huang, W. Liu, X. Li, S. Su, H. Peng, Y. Fang, J. Dong and Q. Sun, *ACS Catal.*, 2025, **15**, 6199.
14 S. Zhao, Y. Zhang, Z. Rao, H. Liu, R. Zhang, W. Jia, J. Zhang, Y. Sun and L. Peng, *Appl. Catal. B: Environ. Energy*, 2025, **371**, 125228.
15 C. Árvai, A. K. Horváth, K. Komka and L. T. Mika, *Chem. Eng. J.*, 2025, **511**, 161550.
16 M. Gu, Q. Zhu, Q. Ren and X. Kong, *Catal. Lett.*, 2025, **155**, 146.

17 R. Balaga, P. Balla, R. Rajendran, S. Kim, N. Arumugam, A. I. Almansour, K. K. Mandari and M. Kang, *Mater. Today Chem.*, 2025, **48**, 102935.
18 T. Kawakami, S. Yamaguchi, S. Suganuma, K. Nakajima, T. Mitsudome and T. Mizugaki, *ACS Sustainable Chem. Eng.*, 2025, **13**, 7994.
19 Q. Tang, X. Sun, Z. Duan, Z. Xiao and X. Liu, *Mol. Catal.*, 2025, **584**, 115261.
20 A. Kumar, D. R. Kanchan, A. Banerjee, B. P. Singh and R. Srivastava, *ACS Catal.*, 2025, **15**, 8239.
21 H. Zhao, X. Liao, H. Cui, W. Liu, H. Luo, Y. Lv and P. Liu, *J. Catal.*, 2025, **450**, 116333.
22 X. Yang, Z. Huang, W. Liu, X. Li, S. Su, H. Peng, Y. Fang, J. Dong and Q. Sun, *ACS Catal.*, 2025, **15**, 6199.
23 M. M. Villaverde, T. F. Garetto and A. J. Marchi, *Catal. Commun.*, 2015, **58**, 6.
24 S. Sitthisa and D. E. Resasco, *Catal. Lett.*, 2011, **141**, 784.
25 S.-y. Xiao, Y.-c. Wu, B.-j. Li, Z.-x. Peng, H.-l. Zhou, G.-H. Liu, S.-k. Wang and X.-s. Wang, *J. Inorg. Organomet. Polym. Mater.*, 2025, **35**, 3607.
26 C. A. Ashwani, P. Subha, L. Yalagandula, C. Len, S. A. Singh and P. Sudarsanam, *Green Chem.*, 2025, **27**, 7820.
27 M. Fu, Z. Shan, M. Zhang, J. Wang, F. Jia, M. Guan, K. Wang, W. Chen, M. Gao, H. Li, L. Ning, X. Liu and H. Yu, *ACS Appl. Nano Mater.*, 2025, **8**, 11002.
28 C. Zhang, Y. Zhang, Y. Li, T. Xu, Y. Sun and J. Bai, *Mater. Res. Bull.*, 2024, **179**, 112946.
29 S. Kumar, M. M. Devi, S. K. Kansal and S. Saravanamurugan, *Catal. Sci. Technol.*, 2020, **10**, 7016.
30 J. Liu, W. Zhang, N. Li, L. Ma and L. Chen, *Waste Biomass Valor.*, 2025, **16**, 6175.
31 J. Zhang, Y. Li, Z. Zhang, Z. Wang, J. Zhang, S. Liu, Y. Qin, B. Zhu, T. Zhang, H. Wang, F. Wang and X. Zhang, *RSC Adv.*, 2025, **15**, 4443.
32 M. Huai, X. Li, Y. Zhang, X. Qin, Y. Zhang, X. Qin, Y. Liu, X. Liang, G. Li and J. Zhao, *ChemCatChem*, 2025, **17**, e202401651.
33 X.-Y. Xiao, J. Zhang, R. Wang, Q. Wang, H.-S. Li and J.-H. Yang, *Biomass Bioenergy*, 2026, **205**, 108566.
34 S. Xu, X. Han, F. Zhang, Z. Sun, R. Chai, F. Xu, S. Du, X. Jiao, D. Chen and J. Zhang, *Chem. Eng. J.*, 2025, **522**, 167587.
35 S. Mishra, N. Kamal, A. K. De, I. Sinha, A. P. Panda, R. K. Dey and R. Bal, *Mol. Catal.*, 2024, **569**, 114617.
36 G. L. D. Rivera, J. O. T. Carlín, C. J. L. Ortiz, T. J. M. Herrera, E. H. Fernández, A. M. Bárcenas, L. S. Rangel and C. S. Maldonado, *MRS Adv.*, 2025, **10**, 923.
37 S. E. Sih, F. F. Duro, C. G. Sancho, F. J. G. Mateos, J. M. Rosas, R. M. Tost, P. M. Torres and J. A. Cecilia, *Top. Catal.*, 2025, **68**, 99.
38 P. A. Kamble, M. L. Kantam and V. K. Rathod, *ChemistrySelect*, 2021, **6**, 6601.
39 J. I. Mohammed, G. M. Marta, O. Amin, C. M. Jinesh, I. A. Mark, J. T. Martin, T. Sotirios and K. Georgios, *Appl. Catal., B*, 2021, **299**, 120652.
40 Z. Yang, X. S. Cong, D. G. Teng, X. Y. Wei, Z. X. Li and H. S. Xie, *Fuel Process. Technol.*, 2023, **239**, 107507.
41 X. R. Ma, Z. G. Zhu, Q. T. Dong, T. R. Kong, X. F. Li, T. Su, B. W. Huang, H. Y. Lü and K. X. Yang, *ACS Appl. Nano Mater.*, 2024, **7**, 26825.
42 A. Z. Wang, K. S. Yao, S. B. Li, Q. Wang, T. H. Han, W. W. Lu and H. L. Zhao, *Int. J. Hydrogen Energy*, 2024, **92**, 624.
43 X. Q. Tian, Y. P. Dong and M. Zahid, *Mol. Catal.*, 2023, **545**, 113188.
44 J. Wang, Y. Quan and J. Ren, *Sep. Purif. Technol.*, 2025, **362**, 131568.
45 J. Wang, J. Yang, Z. Bing, Y. Gao, T. Yang, Q. Liu, M. Zhang and Z. Liu, *Molecules*, 2025, **30**, 225.
46 X. Yang, Z. Chen, J. Tan, Y. Zhang, J. Cui, C. Wang, L. Fang, Y. Zhu, L. Huang, H. Shi and Y. Wang, *Chem. Eng. J.*, 2024, **501**, 157796.
47 Y. Gao, W. Yi, J. Yang, K. Jiang, T. Yang, Z. Li, M. Zhang, Z. Liu and B. Wu, *Molecules*, 2024, **29**, 2753.
48 J. Zhang, X. Yang, Z. Jia, Q. Han, S. Yu, S. Liu, L. Li, Q. Wu, H. Yu, Y. Liu and Y. Liu, *Chem. Eng. J.*, 2024, **500**, 157400.
49 R. Arundhathi, P. L. Reddy, C. Samantaa and B. L. Newalka, *RSC Adv.*, 2020, **10**, 41120.
50 J. Zhang, Y. Li, Zh. Zhang, Z. Wang, J. Zhang, S. Liu, Y. Qin, B. Zhu, T. Zhang, H. Wang, F. Wang and X. Zhang, *RSC Adv.*, 2025, **15**, 4443.
51 Q. Zhang, Y. Li, Z. Pan and G. Wang, *Catal. Lett.*, 2025, **155**, 127.
52 Z. Zhao, X. Li, X. Liu, H. Gao, A. Jia, S. Xie, X. Song, X. Liu, F. Yang and Q. Yang, *ACS Catal.*, 2024, **14**, 4478.
53 J. Zhang and D. Wu, *Mater. Chem. Phys.*, 2021, **260**, 124152.